On the decay of turbulence in the 20-liter explosion sphere

Document Version:
Publisher's PDF, also known as Version of Record (includes final page, issue and volume numbers)

Please check the document version of this publication:

• A submitted manuscript is the version of the article upon submission and before peer-review. There can be important differences between the submitted version and the official published version of record. People interested in the research are advised to contact the author for the final version of the publication, or visit the DOI to the publisher's website.
• The final author version and the galley proof are versions of the publication after peer review.
• The final published version features the final layout of the paper including the volume, issue and page numbers.

Link to publication

On the Decay of Turbulence in the 20-Liter Explosion Sphere

A.E. DAHOE[1,2], R.S. CANT[2] and B. SCARLETT[1]
[1]*Department of Chemical Engineering, Delft University of Technology, Julianalaan 136,*
2628 BL Delft, The Netherlands
[2]*Department of Engineering, University of Cambridge, Cambridge CB2 1PZ, United Kingdom*

Abstract. The transient flow field in the standard 20-liter explosion sphere was investigated by means of laser Doppler anemometry. Velocities were measured at various locations within the flow field, and this information was used to quantify the transient behavior of the root-mean-square of the velocity fluctuations and to investigate the spatial homogeneity and the directional isotropy of the turbulence. The investigation involved the transient flow fields generated by the three most widely used dust dispersion systems, namely, the Perforated Dispersion Ring, the Rebound Nozzle, and the Dahoe Nozzle. With all three dispersion dust devices, the decay of turbulence could be correlated by a decay law of the form

$$\frac{v'_{\mathrm{rms}}}{v'_{\mathrm{rms}}{}^{\circ}} = \left(\frac{t}{t_0}\right)^n .$$

It was found that no formal cube-root-law agreement exists between the 20-liter explosion sphere and the 1-m^3 vessel. The results of this work also call into question the widely held belief that the cube-root-law is a valid scaling relationship between dust explosion severities measured in laboratory test vessels and the severity of industrial dust explosions.

Key words: cube-root-law, dust explosion, laser Doppler anemometry, turbulence decay.

1. Introduction

The safe operation of chemical plants handling combustible particles requires characterization of the severity of an accidental dust explosion under actual process conditions of pressure, temperature and turbulence. In the absence of a comprehensive approach which is capable of predicting the transient combustion behavior of gas-particle flows in industrial plant units, researchers have adopted a practical methodology to assess the severity of an accidental dust explosion. In this methodology dust explosion severity parameters are measured using laboratory test vessels in order to estimate what would happen if the same mixture exploded in an industrial plant unit.

Typical dust explosion severity parameters which form the design basis for a great deal of practical safety in industrial plants are the maximum explosion pressure, P_{max}, and the maximum rate of pressure rise, $(\mathrm{d}P/\mathrm{d}t)_{\mathrm{max}}$. Their practical
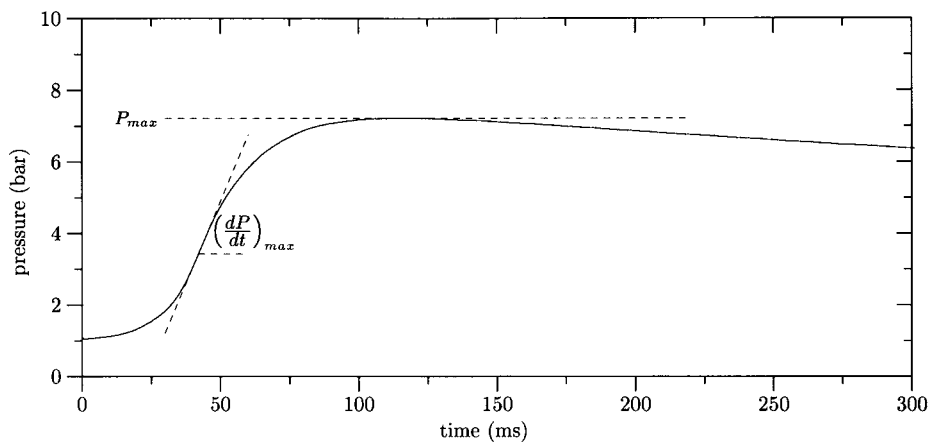
Figure 1. Explosion curve of a 500 g m^{-3} cornstarch-air mixture in the standard 20-liter explosion sphere.

relevance can be understood with the aid of the pressure-time curve of a cornstarch-air dust explosion shown in Figure 1. At the beginning of the explosion the pressure is equal to the atmospheric pressure (1 bar) and increases up to a maximum value of about 7 bar, which marks the end of the explosion process. During the explosion the pressure increases progressively until the rate of pressure rise achieves a maximum, after which the pressure continues to increase with a progressively decreasing rate of pressure rise. The maximum explosion pressure and the maximum rate of pressure rise are both determined from the experimental pressure-time curve as shown by Figure 1. The reasons for choosing these quantities to characterize the severity of an industrial dust explosion are also evident from this figure. The maximum explosion pressure gives an indication of the magnitude of the damaging pressures that may be generated and the maximum rate of pressure rise indicates how fast these pressures can develop. From a practical point of view the maximum explosion pressure may be used to determine the design strength of industrial equipment so that it can withstand the violence of an explosion. The maximum rate of pressure rise may be used to dimension pressure relief systems which counteract the development of damaging pressures so that they do not exceed a particular design strength.

Both the maximum explosion pressure and the maximum rate of pressure rise are known to be a function of the chemical composition, pressure, temperature and flow properties. In case of the maximum explosion pressure, the application of laboratory test data to industrial plant units appears to be straightforward, provided that similar conditions of pressure, temperature, and flow properties exist in the laboratory test vessels and the industrial equipment. The maximum explosion rate of pressure rise, however, requires the use of a scaling law which is known as the cube-root-law [1–3]. In other words, if chemically identical mixtures are ignited to deflagration in two differently sized vessels with identical conditions of pressure,

temperature and turbulence, and changes in these conditions would be the same during the course of an explosion in these vessels, one would measure identical maximum explosion pressures. At the same time, one would find a lower maximum rate of pressure rise in the larger vessel. As this is a consequence of the difference in size between the vessels, researchers have adopted the cube-root-law,

$$K_{St} = \left(\frac{dP}{dt} \right) V^{1/3}, \tag{1}$$

which is to be applied as follows. The maximum rate of pressure rise measured in one vessel (i.e. the laboratory vessel) is multiplied by the cube root of its volume to yield a K_{St}-value which is assumed to be a volume invariant dust explosion severity index. The maximum rate of pressure rise of the same mixture in the other vessel (i.e. plant unit) is obtained by dividing this K_{St}-value by the cube root of its volume. The resulting dust explosion severity then forms the design basis for explosion protection (e.g. explosion relief venting, explosion suppression). This approach is known as the VDI-methodology and rests entirely on the validity of the cube-root-law.

It is the purpose of this paper is to present experimental results which are relevant to two issues in the study and prediction of dust explosion behavior. The first issue concerns the formal cube-root-law agreement which is believed to exist between dust explosion severities measured in differently sized vessels, and hence between dust explosions in small laboratory test vessels and accidental dust explosions on an industrial scale.

Bartknecht [3] presented research which showed that K_{St}-values found using the 20-liter sphere were identical to those found using the 1-m^3 vessel (see Figure 2). This research was initially carried out because the 1-m^3 vessel, which was the only internationally accepted dust explosion testing device (ISO 6184/1 [4]), required much labor and large amounts of powder. With dust concentrations being typically between 0.1 and 1.5 kg m^{-3}, the cost of dust explosion severity testing involving expensive powders (e.g. pharmaceutical compounds) would be greatly reduced by the use of a smaller explosion vessel. Therefore, Siwek [5] developed a 20-liter explosion sphere which requires much less labor and functions with 50 times less powder, and was hailed as a significant advance in powder safety testing. Its acceptance as a standardized dust explosion testing device, however, would depend on whether or not it would give the same K_{St}-values as the 1-m^3 vessel.

A particular problem which had to be overcome was that of the turbulence of the dust clouds which are ignited to deflagration in the test vessels. The origin of this problem stems from the fact that without some degree of fluid motion a dust cloud cannot exist because the particles have a tendency to settle out. With both test vessels an air blast is used to initially suspend the particles, and the turbulence which is generated by the air blast keeps the particles air-borne until ignition occurs. In order to clarify the difficulties posed by this problem it is necessary to consider the method by which the air blast is generated in some detail.
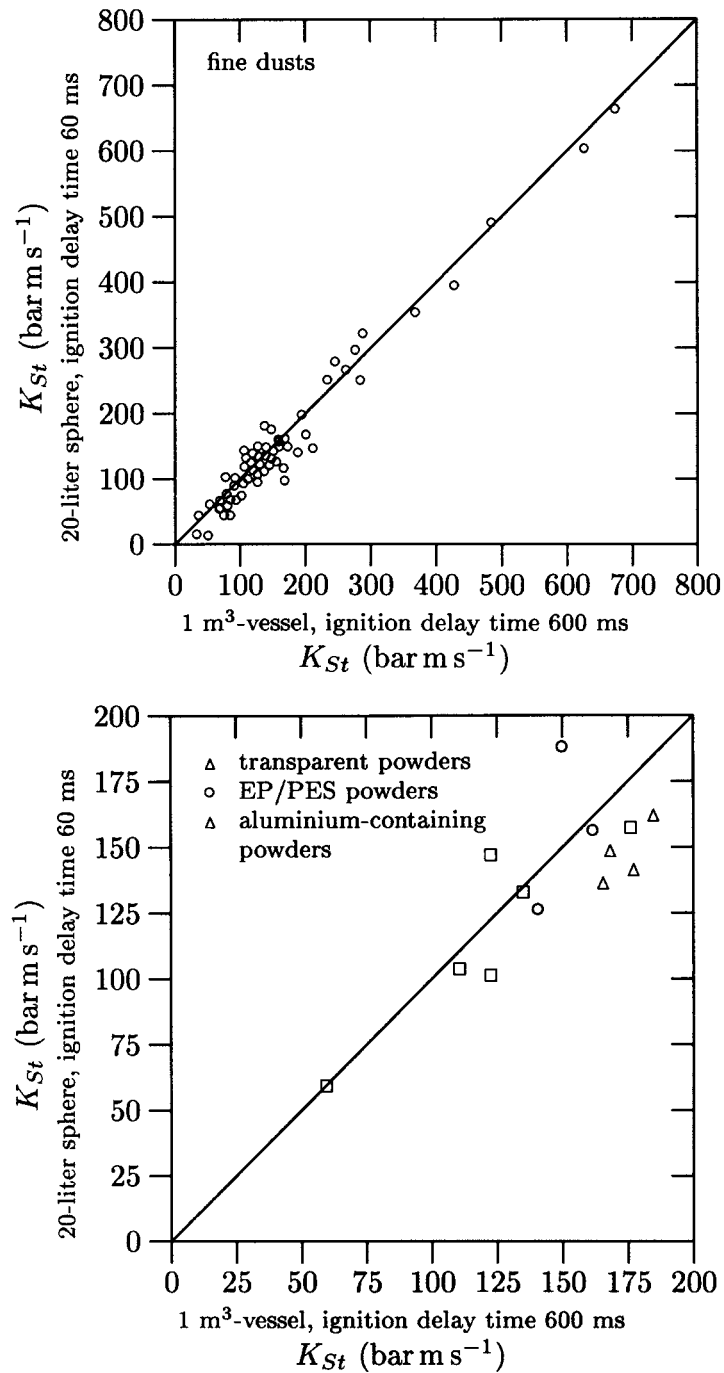
Figure 2. K_{St}-values of various dusts measured in the 1 m^3-vessel and the 20-liter sphere as reported by Bartknecht [3].

In case of the 1-m^3 vessel, two 5.4-liter pressure canisters are mounted on the explosion chamber. These are filled with the dust particles and with compressed air of 20 bar, after which their content is discharged into the explosion chamber. Before the air blast, the pressure in the explosion chamber is made equal to 1 bar and it is only slightly affected by the discharge because the volume of the canisters is comparatively small. The air blast, during which considerable turbulence is generated and a dust cloud is formed in the explosion chamber, lasts 600 ms. Since the burning rate is increased by turbulence, and due to the transient nature of the turbulence level, a practical test procedure was adopted which required that ignition must occur as soon as the air blast is completed. The time between the beginning of the air blast and the moment of ignition is known the ignition delay time. It was assumed that the turbulence level in the 1-m^3 vessel was the highest at an ignition delay time of 600 ms (after this time turbulence decay becomes larger than turbulence production) and that this significant, but unknown, turbulence level would never be exceeded by what might exist in industrial equipment. Dust explosion severity parameters, measured in the 1-m^3 vessel, were therefore believed to be a conservative estimate of what might happen when an accidental explosion occurs in industrial equipment.

In case of the 20-liter sphere, the dust particles and compressed air are discharged into the explosion chamber from a pressure canister with a volume 0.4 liter. The explosion chamber is initially evacuated to a pressure of 0.4 bar and the pressure canister is filled with compressed air of 21 bar. The air blast lasts about 50 ms, after which the pressure in the explosion chamber becomes equal to 1 bar and turbulence starts to decay. As indicated by Figure 2, Bartknecht and Siwek observed that the 20-liter sphere produced K_{St}-values that were in agreement those obtained with the 1-m^3 vessel when the ignition delay time in the former was set equal to 60 ms. This observation did not only give rise to the belief that the turbulence properties in the 20-liter sphere at an ignition delay time of 60 ms were equal to those in the 1-m^3 vessel at an ignition delay time of 600 ms. It also inspired the widespread belief that a formal cube-root-law agreement could exist between turbulent dust explosions in small laboratory test vessels and large scale dust explosions in industrial equipment. In addition to that, technical guidelines adopted the notion that powder safety testing of all types of combustible dusts can be performed using the 20-liter sphere by adhering to a single prescribed test procedure with a single, fixed ignition delay time of 60 ms, and that these results, in conjunction with the cube-root-law, can form the design basis of industrial safety.

In spite of the experimental evidence presented by Bartknecht and Siwek, based on a variety of powders, other researchers questioned the generality of the observation of a formal cube-root-law agreement between the 20-liter sphere and the 1-m^3 vessel. Van der Wel et al. [6], measured the K_{St}-value of potato starch, lycopodium, and activated carbon with both test vessels (see Figure 3), and found that the K_{St}-value in the 20-liter sphere at an ignition delay time of 60 ms was not in agreement with that in the 1-m^3 vessel at an ignition delay time of 600 ms. Instead, they
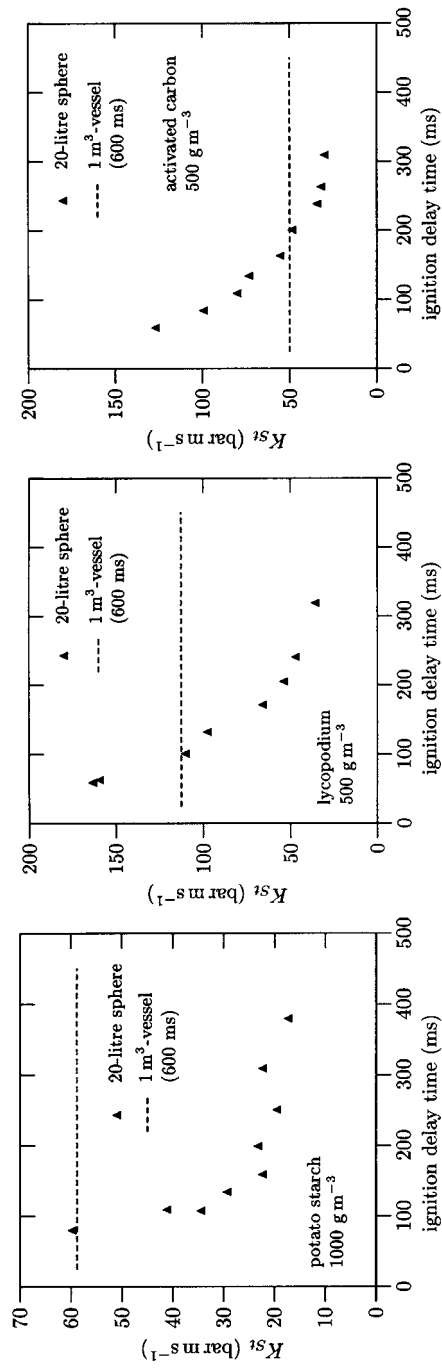
Figure 3. K_{St}-values of various dusts measured in the 1-m^3 vessel and the 20-liter sphere as reported by van der Wel et al. [6].

found that the K_{St}-values in the 20-liter sphere were in agreement at ignition delay times of 80, 100, and 165 milliseconds. Apart from measuring K_{St}-values in the 20-liter sphere at various ignition delay times, and hence different conditions of turbulence, van der Wel et al. used hot-wire anemometry to measure turbulence frequency spectra in both vessels [6]. Although these researchers did not measure the turbulence level in the 20-liter sphere explicitly, their research indicated that conditions of similar turbulence existed in the two vessels when the ignition delay time in the 20-liter sphere was equal to 165 ms, instead of the prescribed 60 ms. A similar observation was also made by Pu et al. [7], who performed explicit turbulence measurements inside the 20-liter sphere by means of hot-wire anemometry. A comparison of their results with those obtained in a 1-m^3 vessel (see Figure 13) indicates that equal turbulence levels exist in both test vessels when the ignition delay time of the 20-liter sphere is 200 ms.

The work of van der Wel et al. and Pu et al. undermines the widespread belief that a formal cube-root-law agreement generally exists between the 20-liter sphere and the 1-m^3 vessel, and that dust clouds are ignited under similar conditions of turbulence when both vessels are operated according to prescribed test procedures. In fact, these observations undermine the entire notion that laboratory test results may be used to predict what would happen under industrial circumstances on the basis of the cube-root-law.

The second issue concerns the abandonment of the VDI-methodology and its replacement by a more accurate and theoretically justified method of prediction. It was pointed out by various researchers [8–10] that the cube-root-law is no more than an approximation of a single realization of the explosion pressure curve and that it is only valid as a scaling relationship under hypothetical circumstances.

First, the mass burning rate (i.e. the product of the burning velocity, the flame area, and the density of the unburnt mixture which is to be consumed by the flame) has to be the same in both the test vessel and the industrial vessel at the moment when the rate of pressure rise reaches its maximum value. This condition is only fulfilled when both vessels are spherical, ignition occurs at the center of both vessels, the flow properties are identical, and changes in pressure, temperature and turbulence of the unburnt mixture ahead of the flame have the same effect on the burning velocity. In reality none of these requirements are fulfilled. In addition to that, laboratory test results, obtained under particular conditions of turbulence, are applied to industrial circumstances where different conditions of turbulence exist. Since the effect of turbulence is not explicitly taken into account by the cube-root-law, its application may lead to unacceptable over-estimations in situations where turbulence levels in industrial practice are much lower than those created in laboratory test vessels, but also to under estimations of the explosion severity under circumstances where additional turbulence is generated by the explosion itself. It was demonstrated by Tamanini [11] that worst case predictions by means of the VDI-methodology may underestimate the dust explosion severity when turbulence varies at the time of the explosion.

Secondly, the thickness of the flame must be negligible with respect to the radius of the vessel. It was demonstrated by Dahoe and co-workers [10, 12] that an inherent limitation of the cube-root-law is that it does not take the effect of flame thickness into account. When the flame thickness is significant with respect to the radius of a laboratory test vessel (i.e. > 1%), the cube-root-law no longer transforms the maximum rate of pressure rise into a volume invariant explosion severity index. Instead, it transforms a laboratory test result into an explosion severity index which systematically underestimates the maximum rate of pressure rise in a larger vessel. Since many powders have a flame thickness that is appreciable with respect to the radius of laboratory test vessels, the cube-root-law may not be considered as generally valid for the prediction of dust explosion severity. With some dusts, the flame thickness is so large that application the cube-root-law irrevocably leads to an underestimation of the maximum rate of pressure rise in larger vessels, even when laboratory testing is carried out at considerably higher turbulence levels.

In order to overcome the limitations associated with the cube-root-law several models have been proposed by other researchers. Unlike the cube-root-law, which takes a single instant of the rate of pressure rise measured in a test vessel to predict a single instant of the rate of pressure rise during an industrial explosion, these so called integral balance models are capable of predicting the entire pressure evolution during an explosion. And, more importantly, since their derivation is based on fundamental relationships between the pressure development and the mass burning rate at any instant, the effect of mixture composition, pressure, temperature, and turbulence on the transient combustion process can be taken into account in an explicit manner. Existing models of this kind are those of Bradley and Mitcheson [13], Nagy and Verakis [14], Perlee et al. [15], and Chirila et al. [16], Bradley et al. [17], Tamanini [18] and Dahoe and co-workers [10, 12]. Ideally, these models enable the prediction of explosion behavior, and hence the explosion severity, under industrial circumstances when the mass burning rate is known from laboratory experiments and the (varying) turbulence parameters are known for industrial circumstances. In the case of premixed gases, the burning velocity and the flame thickness are recognized as fundamental measures of the driving force behind the combustion process and these quantities have been used with success to model the mass burning rate. It is believed that the same approach may be also applied to dust-air mixtures [9, 19].

When the burning velocity and flame thickness are used as key parameters in integral balance models, a distinction is made between a laminar burning velocity and a laminar flame thickness, on one hand, and a turbulent burning velocity and a turbulent flame thickness on the other hand. A great advantage of this distinction is that it separates the effect of mixture properties (chemical,thermodynamical) and the effect of flow properties (turbulence level,turbulence length scale) on the flame propagation process in a systematic way. When, for example, a flame is stabilized in a laminar flow of combustibles, it establishes itself at a fixed position in the flow field and its surface remains smooth. In other words, it inherits the laminar

behavior of the flow field. Moreover, the velocity at which the cold reactants enter the flame zone in the normal direction, the laminar burning velocity, and the width of the region in which reactants are converted into combustion products, the laminar flame thickness, appear to be a mixture specific properties. They reflect the sensitivity of the combustion process to changes in the chemical composition, fuel concentration, oxygen content, particle size, pressure and temperature of the approaching flow of reactants. By contrast, when a flame is trapped within a turbulent flow of combustibles, it inherits the turbulent nature of the flow field: the turbulence of the approaching flow continuously distorts the flame and ceaselessly shifts its position in space between certain geometrical boundaries. As a result, the surface area of the instantaneous laminar flame changes in a chaotic manner which is determined by the turbulence of the flow field. Owing to the fact that the relevant time scales of the fluid structures that compose the turbulent flow field are much larger than the the chemical time scale of the instantaneous combustion zone, the geometrical boundaries between which the instantaneous flame front shifts its position are identified as a turbulent flame thickness. Due to the enhancement of heat and mass transfer by turbulence, the turbulent flame zone propagates with a turbulent burning velocity which is greater than the laminar burning velocity. The local consumption of reactants at any particular portion of the flame surface, however, occurs within a zone whose width is equal to the local laminar flame thickness and at a rate which is determined by the local laminar burning velocity. With this picture in mind, various researchers have developed relationships which express the turbulent burning velocity and the turbulent flame thickness in terms of a combination of the laminar flame propagation parameters and the turbulence features of the flow field.

It was mentioned earlier that integral balance models can be used to replace the VDI-methodology in the prediction of dust explosion behavior. Since integral balance models are capable of predicting the entire pressure development of an explosion, they can be used in conjunction with the above mentioned relationships to determine laminar burning velocity and the laminar flame thickness by regressing them to the pressure-time curve of laboratory experiments, as demonstrated by Dahoe and co-workers [10, 12], provided that the turbulence properties in the laboratory test vessels are known with sufficient accuracy. These fundamental flame propagation parameters can then be used to predict dust explosion behavior in plant units of a simple geometry by means of the same integral balance models, or, in complex geometries using CFD-codes. The success or failure of this approach, however, depends entirely upon our knowledge of the turbulence properties and how they may vary during the course of an explosion in both the laboratory test vessels as well as in industrial pant units.

Based on the foregoing it is evident that quantitative knowledge of turbulence properties inside laboratory explosion test vessels is of critical importance to the modelling and the prediction of dust explosion behavior. Hence, it is the purpose of this paper to present experimental results on the transient turbulence levels in

the 20-liter sphere. Although turbulence in the 20-liter sphere was studied previously there are still a number of shortcomings. First of all, Pu et al. and van der Wel et al. used hot-wire anemometry to measure turbulence. While this technique enables one to quantify turbulence levels and to measure power density spectra, it is incapable of measuring independent velocity components simultaneously. As a result, it is not possible to investigate whether practically isotropic turbulence, or, a situation of highly non-isotropic turbulence exists in the 20-liter sphere. In order to overcome this limitation a two dimensional laser Doppler anemometer was used in this work. Secondly, previous research was limited to measurements at the geometric center of the 20-liter sphere and ignores the question of whether or not similar conditions of turbulence exist at other locations in the 20-liter sphere. In the present work turbulence measurements are performed at various locations in the flow field. Thirdly, the work by previous researchers is restricted to the investigation of the flow field generated by one specific dust dispersion device, namely, the Perforated Dispersion Ring. Since the dispersion behavior of particles differs from one powder to another, dust explosion severity testing involves the use of a variety of dust dispersion devices. In the present work, the flow fields of three of the most widely used dust dispersion devices, namely, the Perforated Dispersion Ring, the Rebound Nozzle and the Dahoe Nozzle, are investigated. Fourthly, there appears to be a discrepancy between the results of van der Wel et al. and Pu et al. It was observed by van der Wel et al. that conditions of turbulence, similar to those in the 1-m^3 vessel, exist in the 20-liter sphere when the ignition delay time is equal to 165 ms. A comparison between the results of Pu et al. and the turbulence level in the 1-m^3 vessel, however, shows that this ignition delay time should be equal to 200 ms. Since this discrepancy is significant in comparison with the prescribed ignition delay time of 60 ms, and knowing that turbulence decays rapidly after completion of the air blast, it would be interesting to measure turbulence levels in the 20-liter sphere with a technique which is different from the one used by Pu et al. and van der Wel et al., and to compare these results with the turbulence level in the 1-m^3 vessel.

2. Measurement of Turbulence Levels in the 20-Liter Sphere

Due to the limited optical access of the actual explosion chamber, a plastic replica containing optical quality glass windows was constructed and mounted on the commercially available injection section. The transient flow fields were created by means of a blast of compressed air according to the prescribed test procedure for powder safety testing with the 20-liter sphere. This means that the pressure canister was pressurized up to 21 bar, the sphere was evacuated to a pressure of 0.4 bar, and the contents of the canister was subsequently discharged into the sphere. A two dimensional laser Doppler anemometer was used to measure the velocity at various locations in the transient flow field. The details of the laser Doppler anemometer and its implementation are omitted here and can be found in [12]. It is sufficient to
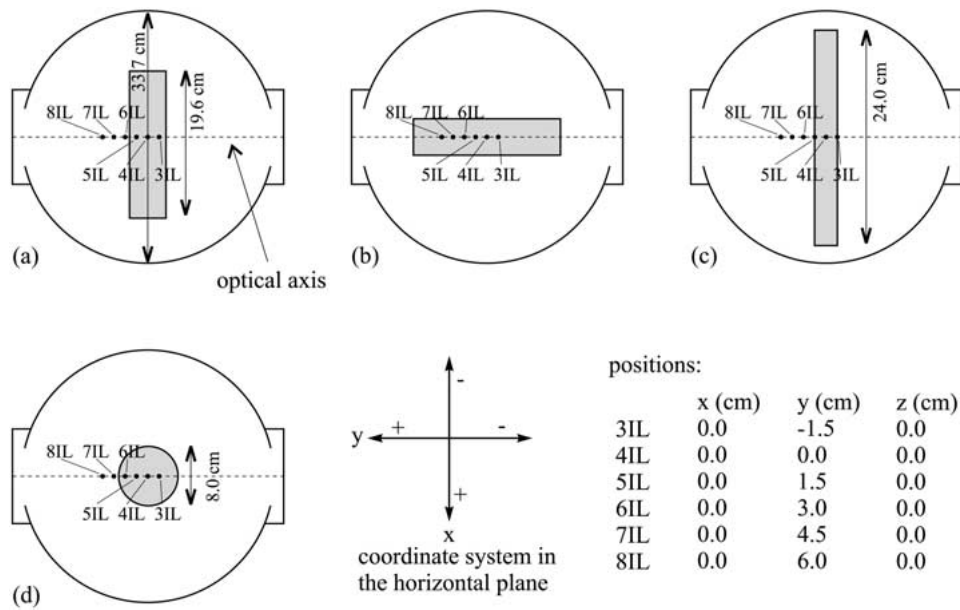
Figure 4. An overview of the measuring locations with (a) the Rebound Nozzle (perpendicular to optical axis), (b) the Rebound Nozzle (parallel to optical axis), (c) the Perforated Dispersion Ring, and (d) the Dahoe Nozzle.
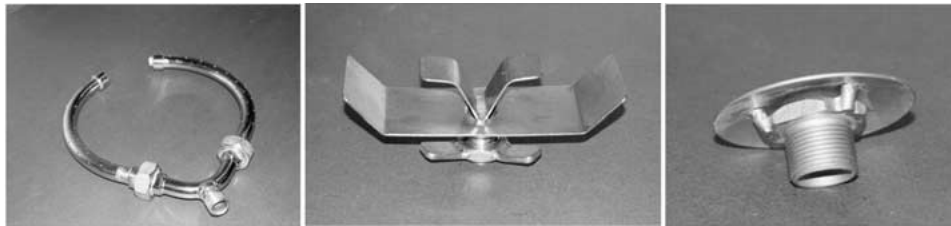

Figure 5. The Perforated Dispersion Ring (left), the Rebound Nozzle (middle) and the Dahoe Nozzle (right).

mention here that the equipment was capable of measuring vertical and horizontal velocity components between -250 m s^{-1} and $+250$ m s^{-1}, and that data rates of up to 25 kHz were observed (i.e. time scales down to 0.02 ms could be resolved).

The vertical and horizontal components of the instantaneous velocity were measured in the transient flow fields generated by three of the most widely used dust dispersion devices, namely, the Perforated Dispersion Ring, the Rebound Nozzle, and the Dahoe Nozzle (see Figure 5). Measurements were performed at six measurement locations and in order to have a sufficient amount of data for statistical averaging, at least ten time series were measured at each location. The measurement locations and the placement of the dust dispersion devices in the model sphere are shown in Figures 4 and 6. All dust dispersion devices are attached to the inlet through which compressed enters the model sphere and the shaded regions
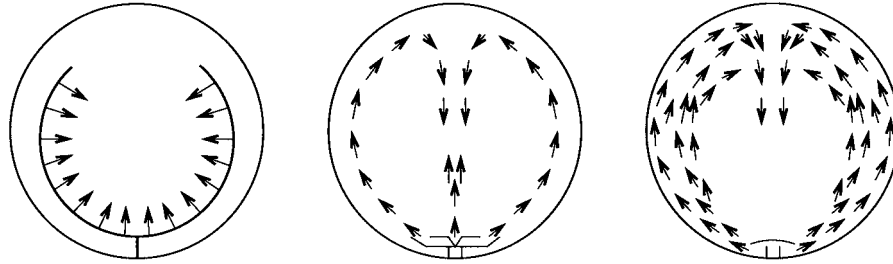
Figure 6. Placement and initial flow patterns of the Perforated Dispersion Ring (left), Rebound Nozzle (middle) and the Dahoe Nozzle (right).

in Figure 4 depict projections of these devices onto the equitorial plane of the model sphere. The six measurement locations, 3IL, 4IL, 5IL, 6IL, 7IL, and 8IL, are situated within the equitorial plane and along the optical axis of the beams emitted by the laser Doppler anemometer. Their relative position with respect to the dust dispersion devices is also indicated by Figure 4.

A few examples of the instantaneous velocity components measured at the geometric center of the model sphere are shown in Figure 7. In the initial stage of the flow field generated by the Perforated Dispersion Ring, the vertical velocity component is seen to oscillate rapidly between -60 and 50 m s^{-1} with no systematic preference for a specific direction. At the same time the horizontal component varies between -50 and 40 m s^{-1}, with a clear preference for the negative horizontal direction in the beginning, followed by a preference for the positive horizontal direction. Both velocity components are observed to decrease to a fraction of their initial magnitude within a period of about 60 milliseconds. With the Rebound Nozzle, the vertical velocity component is observed to vary between -60 and 100 m s^{-1} with a preference for the positive vertical direction. At the same time, the horizontal velocity component changes its magnitude between -45 and 40 m s^{-1}. During the injection process, the initial preference for the positive horizontal direction is seen to change into a preference for the negative horizontal direction. After a period of about 60 milliseconds, both velocity components exhibit a low frequency oscillatory behavior. The velocity components associated with the Dahoe Nozzle show a similar behavior, except that the vertical velocity component varies between -30 and 125 m s^{-1}. The horizontal component lies between -60 and 30 m s^{-1} with a systematic preference for the negative horizontal direction.

In spite of the wild and spiky behavior of the instantaneous velocity, one may still discern a mean motion with relatively large time scales. With the Perforated Dispersion Ring, the mean motion appears to exist only during the first 60 milliseconds of the injection process, which is about equal to the time needed to discharge the contents of the storage vessel into the model sphere. With the Rebound Nozzle and the Dahoe Nozzle, there appears to be a sinusoidal mean motion with a decreasing amplitude and frequency, which persists beyond the discharge time. This is in spite of the fact that the driving force (i.e. the pressure difference
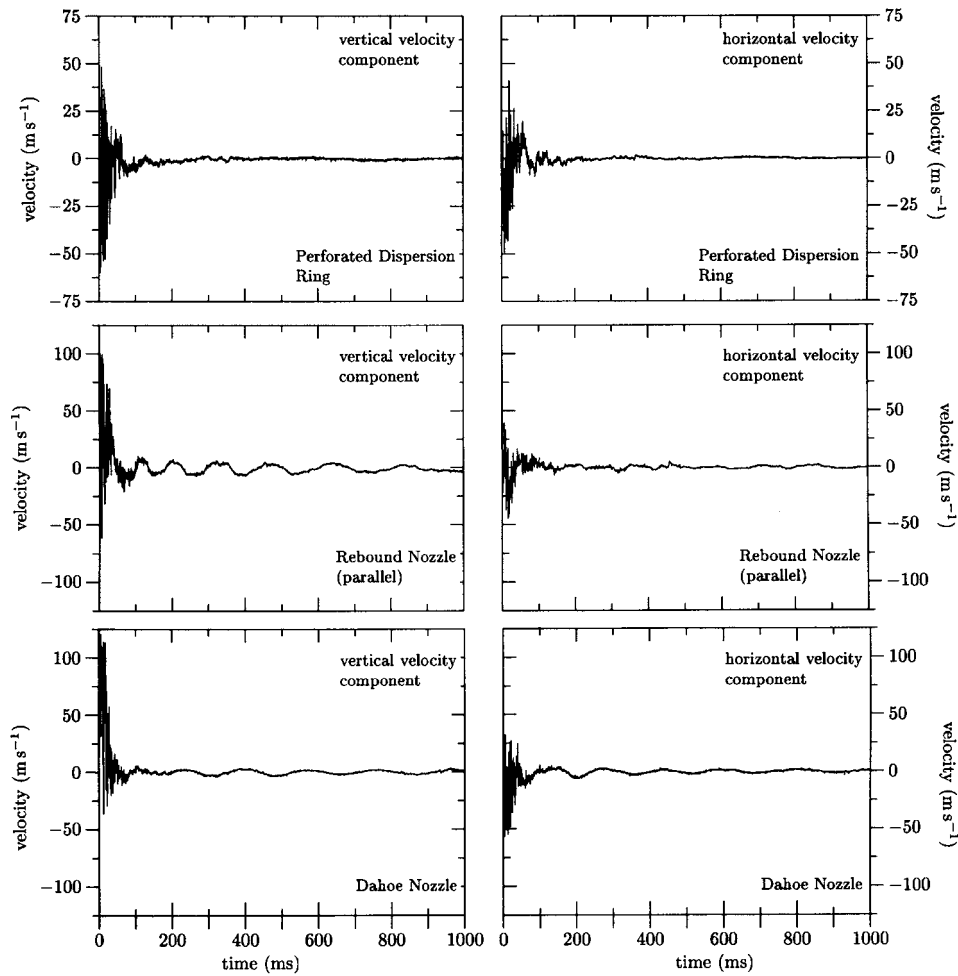
Figure 7. The vertical and horizontal component of the instantaneous velocity at the geometric center of the sphere (location 4IL).

between the storage vessel and the model sphere) is no longer present after the first 60 milliseconds. According to Figure 6 this behavior must be attributed to the initial flow patterns of the dust dispersion devices. During the injection process, the Rebound Nozzle and the Dahoe Nozzle produce large jets which sustain their high velocity and preferential direction for a longer period of time. Since the Perforated Dispersion Ring consists of a metal tube with 112 holes of 3 mm diameter each, the fluid enters the model sphere in the form of a large number of thin jet streams that lose their initial velocity and preferential direction rapidly.

Due to the presence of a mean motion, every realization of the instantaneous velocity had to be decomposed into a mean value and a fluctuation in order to quantify the transient turbulence level in the 20-liter sphere. The mean value was
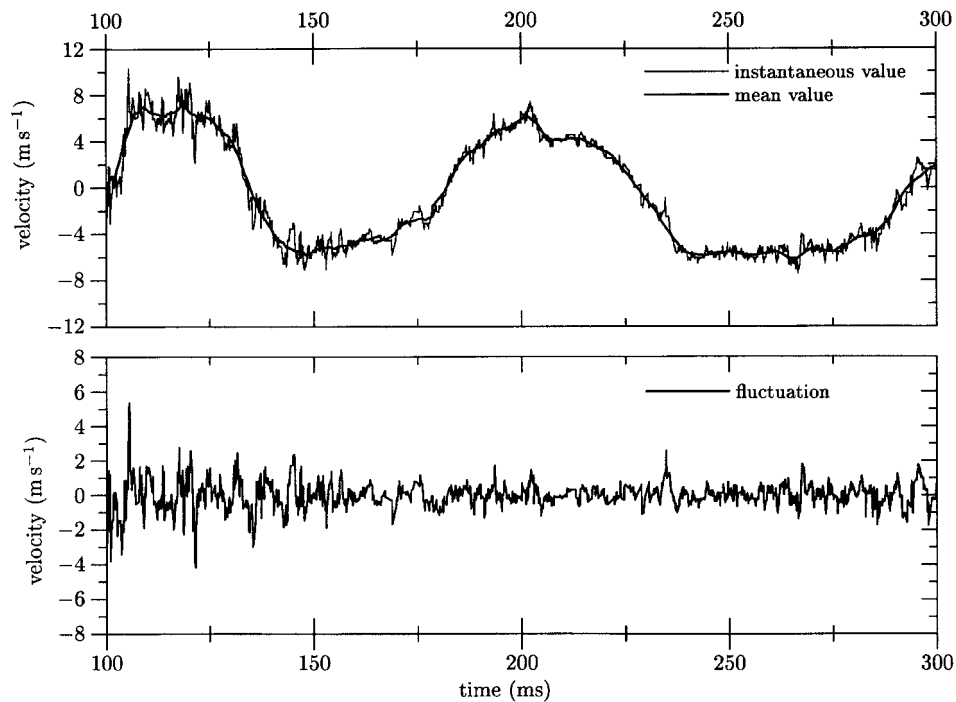
Figure 8. Decomposition of the vertical velocity component into a mean value (top) and a fluctuation (bottom). The instantaneous value corresponds to the result presented in middle-left part of Figure 7.

determined by means of a moving regression routine which fits a polynomial of a particular degree to a data window. The routine picks a sample record of a particular length, say $(t_1, v_1), \ldots, (t_i, v_i), \ldots, (t_n, v_n)$, fits the polynomial to the data set, uses the regression coefficients to calculate the value of the polynomial at each t_i, shifts the data window with one sample, and repeats the process all over with another sample, until all data are processed. The values of the fitted curve at the various values of t_i are an estimation of the mean motion, and subtracting them from the instantaneous values, v_i, yields the velocity fluctuations. The effect of this routine in decomposing a velocity data set into a mean value and a fluctuation is shown by Figure 8.

In principle, the moving regression algorithm can be used with two kinds of data windows. The first, which is called here a point-window, consists of a fixed number of points. The second is called a time-window and consists of a number of samples contained within a fixed time interval. If the data rate would be constant, both windows would be identical with a fixed number of samples covering a fixed time duration. In the case of laser Doppler anemometry, however, where the data rate is not constant (it increases when the velocity increases and vice versa), a point-window covers a variable time interval, and a time-window includes a variable number of samples. Since the use of a time-window involves the risk of containing
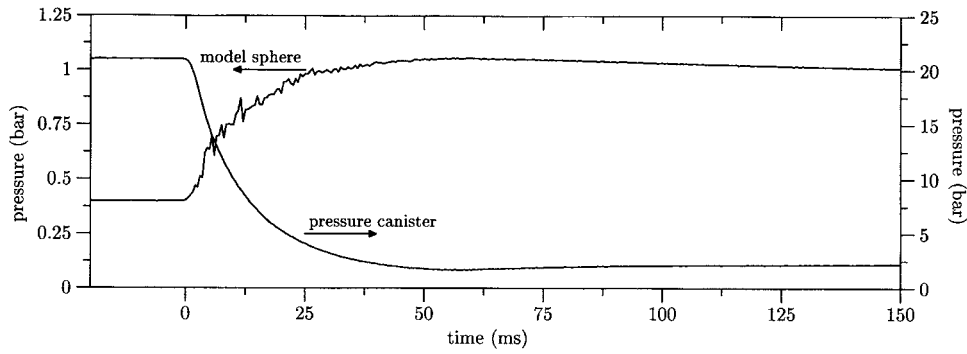
Figure 9. Behavior of the pressure in the model sphere (with the Rebound Nozzle) and the canister during the air blast.

too few points to compute the average, a point-window was used. In this way the algorithm adapted itself to the behavior of the flow: if the velocity decreased, samples were taken from a larger time interval so that the averaging was always performed with a large number of samples.

The size of the point-window, as well as the degree of the polynomial, are of great importance. If the point-window is too small, the mean motion can not be resolved because the moving regression will follow the fluctuations. A point-window which is too large will lead to a flattened-out average, and the mean motion will appear in the fluctuation. When the degree of the fitting polynomial is too high, it tends to follow behavior of the fluctuations instead of the trend of the mean motion. This results in an underestimation of the fluctuations. The optimal choice was found to be a point-window with 71 points (35 points to the left and 35 points to the right of the point where the mean motion is to be estimated) and a second degree polynomial. All velocity-time recordings, similar to the ones presented in Figure 7, were processed with these settings. After subtraction of the mean motion from the instantaneous velocity, the fluctuation of the latter (see the lower part of Figure 8) was used to quantify and compare the turbulent flow fields generated by the different dust dispersion devices.

The behavior of the root-mean-square value of the vertical and the horizontal velocity component at the six different measuring locations is shown in Figure 10. Each data point in this figure is the result of at least ten measurements and was determined as follows. The fluctuation of each velocity-time recording was calculated as described above and the time axis was subdivided into equal time slices of 4 ms. The root-mean-square value associated with each time slice was subsequently calculated by combining the corresponding data of all velocity fluctuations at a particular location and by applying

$$
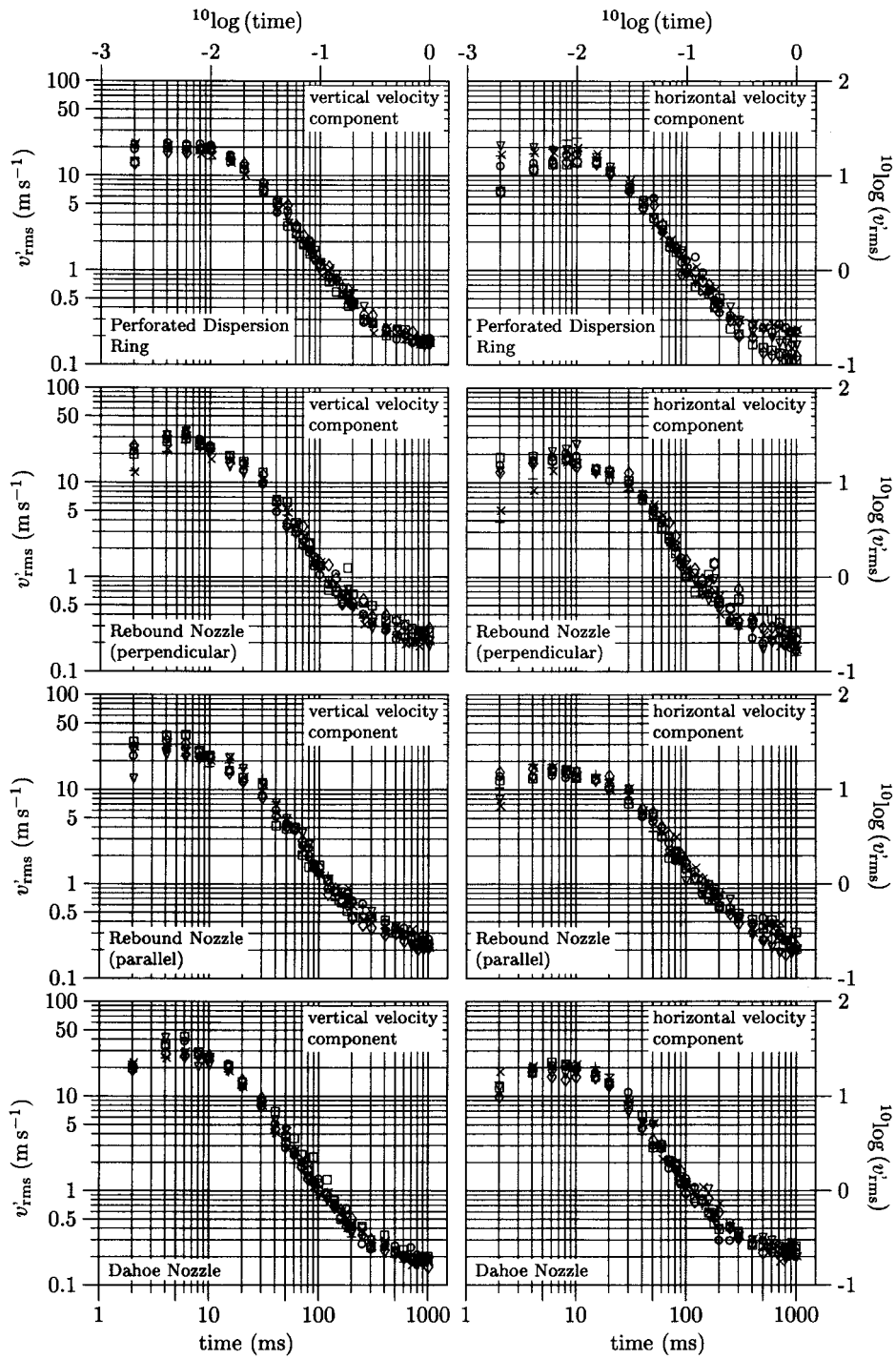v'_{\mathrm{rms}} = \sqrt{\frac{1}{N} \sum_{i=1}^{N} v_i'^2}.
\tag{2}
$$

Figure 10. Root-mean-square values of the velocity fluctuations at the various measuring locations (◇ 8IL, □ 7IL, ○ 6IL, ▽ 5IL, × 4IL, + 3IL) in the 20-liter sphere.

In this equation, v'_{rms} denotes the root-mean-square value, N the total number of samples in each time slice and v'_i stands for the fluctuation of the instantaneous velocity. The resulting v'_{rms}-value was finally assigned to the center of each corresponding time slice.

The spatial homogeneity and directional isotropy of the turbulent flow fields generated by the injection process may be considered by means of Figures 10 and 11. According to Figure 10 the root-mean-square value of both the vertical and the horizontal velocity component, measured at various locations in the model sphere have converged towards each other with all three dust dispersion devices at 60 ms. This implies that homogeneous turbulence exists in the 20-liter sphere at the prescribed ignition delay time of 60 ms, and thereafter. Figure 11 shows the behavior of the space averaged root-mean-square value of the vertical and horizontal velocity fluctuations. Each point of this figure belongs to a time slice of 4 ms and was calculated by superimposing all the corresponding velocity fluctuations, measured at all six locations, and by applying Equation (2). It is seen that the initially different v_{rms}-values of the vertical and the horizontal velocity components have converged to more or less the same value at the prescribed 60 ms. Hence, conditions of practically isotropic turbulence exist in the 20-liter sphere with all three dust dispersion devices. The associated turbulence level at the prescribed ignition delay time of 60 ms is respectively equal to 2.68 m s^{-1}, 3.75 m s^{-1} and 2.79 m s^{-1} in case of the Perforated Dispersion Ring, the Rebound Nozzle and the Dahoe Nozzle.

3. Decay of Turbulence in the 20-Liter Sphere

In order to correlate the transient turbulence level in the 20-liter sphere it is helpful to consider the decay of grid generated turbulence, of which the earliest extensive measurements were made by Batchelor and Townsend [20–22]. These researchers passed a stream of air with a uniform velocity profile through a regular grid of bars and studied the behavior of the velocity fluctuations at the downstream side of the grid. They observed that within a region of up to ten times the mesh spacing, the magnitude of the velocity fluctuations at the downstream side of the grid was increasing to a maximum. It was also observed that within this region, the root-mean-square value of the individual velocity components became independent of position across the stream, and approximately equal to each other. After this region, the magnitude of the velocity fluctuations was found to decay with distance while the turbulence remained homogeneous and isotropic. Batchelor and Townsend distinguished various stages of the decay process and classified them as the initial period of decay, the transition period of decay, and the final period of decay. In all cases the decay of turbulence could be generalized and correlated by means of an equation of the form

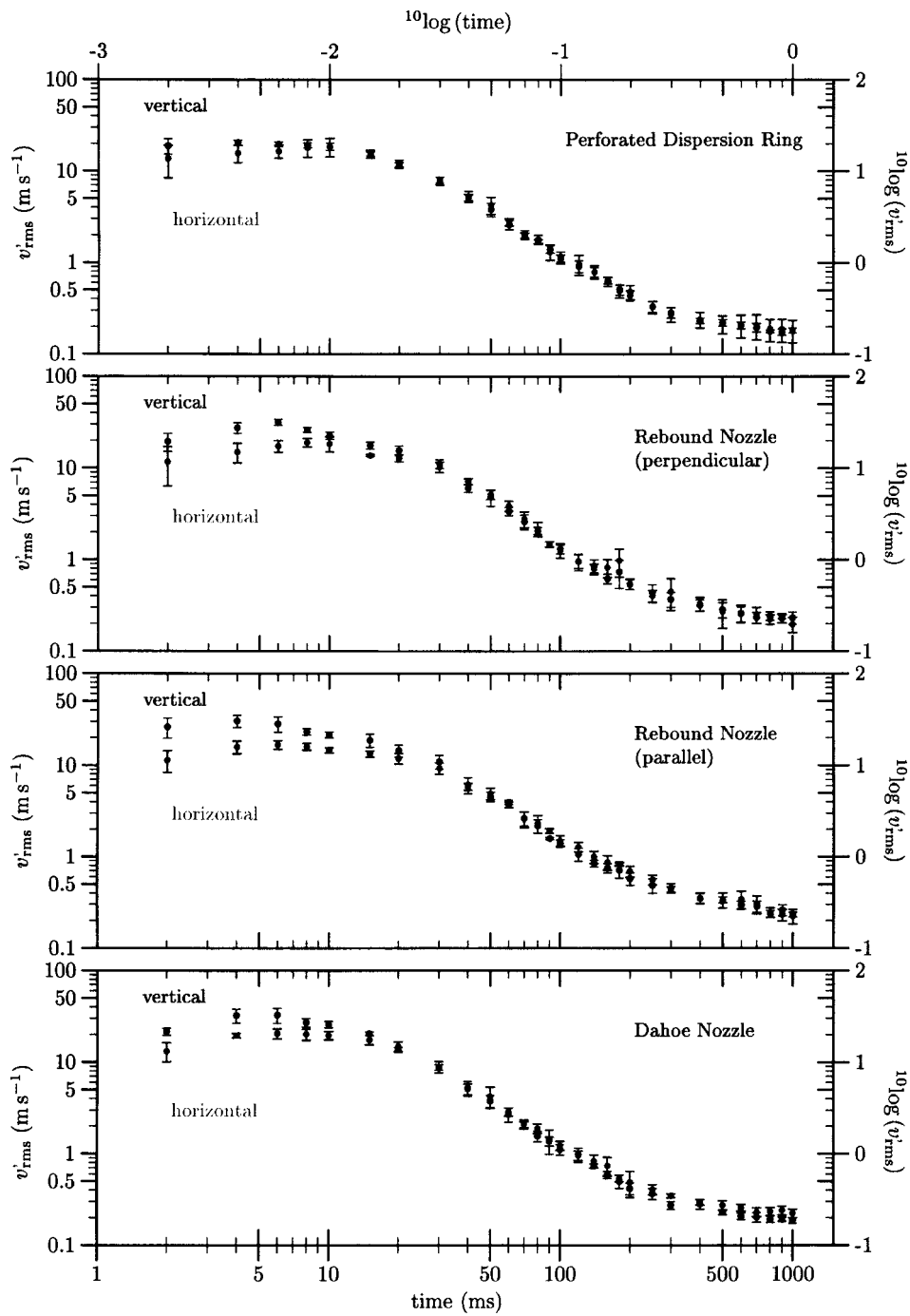$$\frac{v'_{rms}}{v'_{rms}{}^{\circ}} = \left(\frac{t}{t_0}\right)^n,$$

(3)

Figure 11. Space averaged root-mean-square values.

where the distance from the grid at the downstream side is represented by a time coordinate, t (this was accomplished by dividing distance by the mean velocity of the flow). In the initial and final period of decay the exponent, n, was observed to have a constant value of respectively -1.0 and -1.25. In the transition period of decay the exponent, n, was found to change gradually from -1.0 to -1.25.

The turbulent flow field in the 20-liter sphere appears to behave in a similar way. Figure 10 shows that with all three dust dispersion devices the prescribed ignition delay time of 60 ms is preceded by an initial period of turbulence buildup, followed by a period of turbulence decay. According to Figures 10 and 11, a strongly non-homogeneous and anisotropic turbulent flow field is produced in an initial period of about 10 ms. In this period the scatter in the v'_{rms}-value measured at different locations is in the order of 10 m s^{-1}, and a difference of the same order of magnitude can be observed in the v'_{rms}-value of the independent velocity components. As time elapses the turbulent flow field becomes more and more homogeneous and isotropic. At 60 ms both the scatter and the difference between the v'_{rms}-value of the independent velocity components are in the order of 1 m s^{-1}, and this decreases further to 0.1 m s^{-1} at 1000 ms. Although the injection process lasts about 50 ms (Figure 9 shows that the pressure in the model sphere and the canister become equal at about 50 ms), it is seen that turbulence buildup occurs only in an initial period of about 10 ms, and that the decay of turbulence begins to occur while there is still an injection flow of compressed air. In order to understand why the buildup of turbulence is restricted to the first 10 ms, and why turbulence starts to decay while the injection flow is still active, it is helpful to consider the various mechanisms of turbulence generation which are active during the air blast.

The first mechanism may be inferred from the vorticity equation,

$$\frac{\partial \boldsymbol{\omega}}{\partial t} + \boldsymbol{v} \cdot \nabla \boldsymbol{\omega} = \boldsymbol{\omega} \cdot \nabla \boldsymbol{v} + \nu \nabla^2 \boldsymbol{\omega} - \boldsymbol{\omega} \cdot \boldsymbol{v} + \frac{\nabla \rho \times \nabla p}{\rho^2}, \tag{4}$$

where $\boldsymbol{\omega} = (1/2) \nabla \times \boldsymbol{v}$ denotes the vorticity, $\boldsymbol{v}$ the velocity vector, ρ the density, p the pressure, and ν the kinematic viscosity. Prior to the injection process, the storage canister is filled with compressed air of 21 bar (this has a density of about 27 kg m^{-3}), and the model sphere is evacuated to a pressure of 0.4 bar (and the air inside the sphere has a density of about 0.5 kg m^{-3}). When these values are taken into consideration, it is evident that the baroclinic term in the vorticity equation, $(\nabla \rho \times \nabla p)/\rho^2$, must be regarded as a very strong source of vorticity during the injection process. If the length of the duct (which is about 10 cm) that separates the contents of the pressure canister from the contents of the model sphere is taken as a measure of the distance across which the pressure gradient and density gradient exist, and the gradients are assumed to be perpendicular to each other at every fluid element present inside the duct, one finds a vorticity production rate, $\partial \boldsymbol{\omega}/\partial t$, of about $3 \cdot 10^6$ s^{-2} at the very beginning of the injection process. If this situation were to last for only a millisecond, then the initially static state of each fluid element would change into a rotating state of about 3000 cycles per second. In practice, of
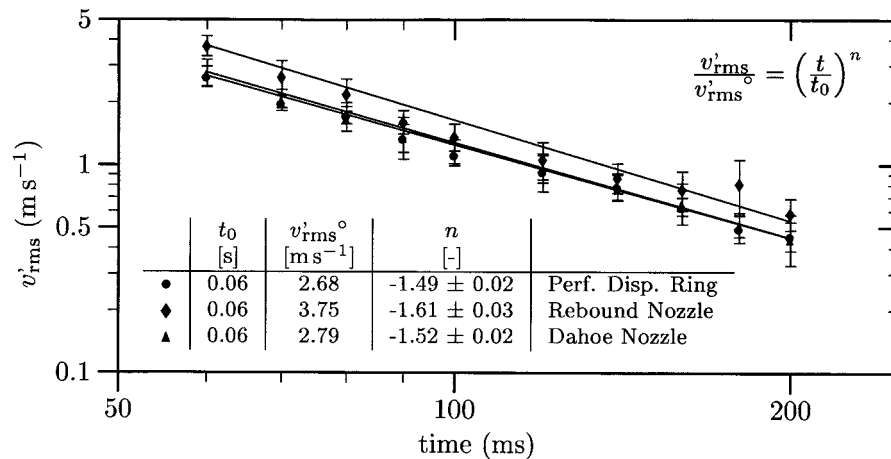
$$\frac{v'_{\mathrm{rms}}}{v'_{\mathrm{rms}}{}^{\circ}} = \left(\frac{t}{t_0}\right)^n$$

	t_0 [s]	$v'_{\mathrm{rms}}{}^{\circ}$ [m s^{-1}]	n [-]	
●	0.06	2.68	-1.49 ± 0.02	Perf. Disp. Ring
♦	0.06	3.75	-1.61 ± 0.03	Rebound Nozzle
▲	0.06	2.79	-1.52 ± 0.02	Dahoe Nozzle

Figure 12. Decay of the root-mean-square velocity from 60 to 200 milliseconds in the 20-liter sphere.

course, the pressure gradient and density gradient are not always perpendicular to one another at every fluid element, and decrease rapidly. This estimate nevertheless gives a reasonable impression of the vigorousness associated with the discharge of the contents of the pressure canister into the model sphere. The second mechanism of turbulence generation during the injection process is by wall friction. On its passage from the canister to the model sphere, the air flows at almost sonic velocities through the duct and subsequently past the dispersion device, and turbulence is generated by friction with the wall. The third mechanism is that of shear turbulence. The air streams emerging from the dust dispersion devices enter the model sphere with a preferential direction and at high velocities, and the associated sliding and shearing of fluid layers is a source of turbulence.

Of all three mechanisms, the baroclinic effect in the region where high pressure and low pressure air are initially separated is considered to be the most important because it constitutes a source of turbulence which is much stronger than wall friction or the shearing of fluid layers. In the first 10 ms the baroclinic effect produces a large amount of turbulence which starts to decay when the pressure and density gradient have decreased. During this decay process, the mechanisms of turbulence generation by wall friction and sliding fluid streams continue to produce turbulence. This additional turbulence, however, is insufficient to counteract and to overcome the decay of the turbulence produced by the baroclinic effect. After the first 50 ms, turbulence generation by wall friction is practically absent because there is no longer a flow from the pressure canister to the sphere. The contribution of shear turbulence is also small after this time because the fluid streams that emerge from the dust dispersion devices lose their initial velocity rapidly.

When the decay of turbulence in the 20-liter sphere (i.e. Figure 11) is compared with the decay of grid generated turbulence, as observed by Batchelor and
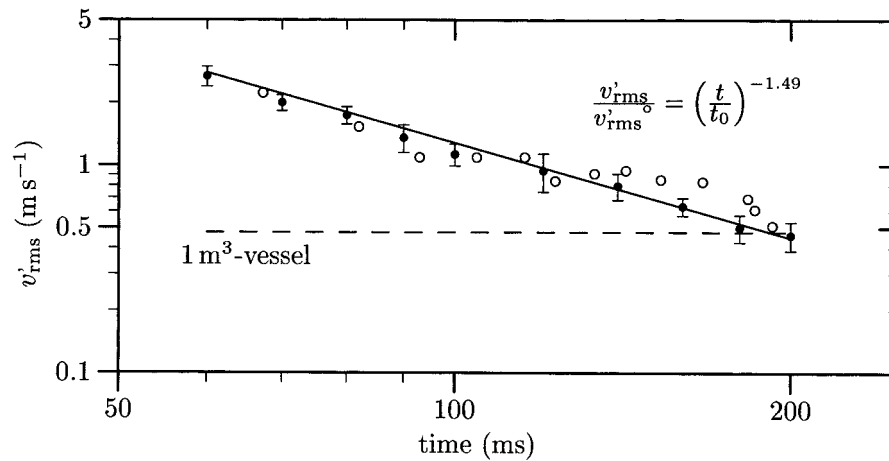
Figure 13. Decay of the root-mean-square velocity in the 20-liter sphere with the Perforated Dispersion Ring ($\bullet$ our measurements, $\circ$ Pu et al. [7], dashed line: 1-m^3 vessel at the prescribed ignition delay time of 600 milliseconds [23]).

Townsend, it is seen that in the period of 10 ms to 50 ms the exponent, n, in Equation (3) gradually decreases to a constant value, as indicated by Figure 12, and that it remains at this constant value until 200 ms. After this time, the exponent increases gradually and tends to become equal to zero. Both behavior and the value of the exponent, n, appear to be different from what has been observed during the decay of grid generated turbulence. The most striking difference is that the decay process of grid generated turbulence consists of two periods in which the exponent, n, assumes a constant value, while the decay of turbulence in the 20-liter sphere involves only one such period. Moreover, the decay exponent in case of the 20-liter sphere assumes a systematically larger (negative) value than the ones observed during the initial and final period of the decay of grid generated turbulence. The reasons for this discrepancy must be sought in the fact that the turbulent fluctuations in the 20-liter sphere are generated by a different mechanism, namely, the baroclinic effect, as described earlier. In the case of grid generated turbulence, friction between the fluid and the grid is the predominant mechanism of turbulence.

In order to have a quantitative description of the behavior of the turbulence level in the 20-liter sphere, our results in the period of 60 to 200 ms were correlated by means of Equation (3). The reason for choosing this time interval was that the decay exponent assumes a constant value and that the explosion times of dust-air mixtures in the 20-liter sphere, ignited at an ignition delay time of 60 ms, rarely exceed 100 ms. According to Figure 12, the constants $v_{rms}'^{\circ}$ and n in Equation (3) assume the values of 2.68 m s^{-1} and -1.49 with the Perforated Dispersion Ring, 3.75 m s^{-1} and -1.61 with the Rebound Nozzle, and 2.79 m s^{-1} and -1.52 with the Dahoe Nozzle. In all cases the constant t_0 has a value of 60 ms. The data points associated with the Rebound Nozzle were calculated in the same manner as those

in Figure 11, except that the measurements with the Rebound Nozzle parallel and perpendicular to the optical axis were combined.

Apart from reducing the volume of the explosion chamber, the development of the 20-liter sphere also involved the development of a dust dispersion device that was to be used in the new vessel. Since the 1-m^3 vessel uses a perforated half-ring with 13 holes of 6 mm diameter each to disperse the dust, a Perforated Dispersion Ring was designed for the 20-liter sphere which consists of a perforated half-ring with 112 holes of 3 mm diameter each. As this device did not work well with a large number of dusts, an alternative device was developed, namely, the Rebound Nozzle, which gave the same K_{St}-value as the Perforated Dispersion Ring. The results presented in Figure 12, however, show that these identical K_{St}-values were measured under significantly different conditions of turbulence using the two dust dispersion devices. At the prescribed ignition delay time of 60 ms, the turbulence level generated by the Rebound Nozzle is a factor 1.4 larger than that generated by the Perforated Dispersion Ring. The turbulence levels produced by the Dahoe Nozzle, on the other hand, are in close agreement with those produced by the Perforated Dispersion Ring.

Figure 12 shows a comparison between our turbulence measurements in the 20-liter sphere with the Perforated Dispersion Ring and the turbulence measurements reported by Pu et al. It is seen that our results, obtained by means of laser Doppler anemometry, are in agreement with those obtained by Pu et al., who used hot-wire anemometry to measure turbulence. The turbulence level in the 20-liter is also compared with the turbulence level in the 1-m^3 vessel at the prescribed ignition delay time of 600 ms. According to this comparison, the turbulence level in the 20-liter sphere is equal to that in the 1-m^3 vessel when the ignition delay time is equal to 200 ms, instead of the prescribed 60 ms. This result contradicts the observation made by van der Wel et al., namely, that similar conditions of turbulence exist in both vessels when the ignition delay time in the 20-liter sphere is equal to 165 ms.

It was mentioned in the Introduction that the 20-liter explosion sphere would only be accepted by technical guidelines for powder safety testing if it would produce the same K_{St}-values as the 1-m^3 vessel. Hence, Barknecht and Siwek performed extensive measurements, involving a variety of powders, and found that this was indeed the case when the 20-liter sphere was operated with an ignition delay time of 60 ms. According to our turbulence measurements, these K_{St}-values were produced at a turbulence level in the 20-liter sphere which is significantly different from that in the 1-m^3 vessel. In other words, the 20-liter sphere was used to produce K_{St}-values that were equal to those measured in the 1-m^3 vessel by varying the ignition delay time and by making use of the fact that the combustion rate changes with turbulence.

4. Conclusions

Laser Doppler anemometry was used to measure the turbulence level in the 20-liter explosion sphere. Two independent velocity components were measured simultaneously at six different locations in the flow fields generated by the three most widely used dust dispersion devices, namely, the Perforated Dispersion Ring, the Rebound Nozzle and the Dahoe Nozzle. A moving regression algorithm was used to decompose the instantaneous velocity components into a mean value and a fluctuation, and the latter was used to quantify the turbulence level. Our results on the turbulence level in the flow field generated by the Perforated Dispersion Ring are in agreement with the results reported by Pu et al., who used hot-wire anemometry to measure turbulence in the 20-liter sphere.

During the injection process with the Perforated Dispersion Ring the instantaneous vertical velocity component varies between -60 and 50 m s^{-1}, and the instantaneous horizontal velocity component lies between -50 and 40 m s^{-1}. With the Rebound Nozzle, the vertical velocity component is observed to vary between -60 and 100 m s^{-1}, and the horizontal velocity component changes its magnitude between -45 and 40 m s^{-1}. The highest instantaneous velocity components were found with the Dahoe Nozzle. In this case the vertical velocity component was found to range from -30 to 125 m s^{-1}, and the horizontal velocity component was between -60 and 30 m s^{-1}. The lower instantaneous velocities associated with the Perforated Dispersion Ring and the higher velocities observed with the other two dispersion systems can be ascribed to the different geometries and the consequential difference in the fluid streams that emerge from them.

The turbulent flow fields generated with all three dust dispersion devices were found to be spatially homogeneous and directionally isotropic at the prescribed ignition delay time of 60 milliseconds, as well as thereafter. The spatial homogeneity follows from the fact that the root-mean-square values of the velocity fluctuations measured at different locations converge towards each other. The establishment of directional isotropy follows from the observation that the root-mean-square values of the horizontal and vertical velocity fluctuations converge to each other. At the prescribed ignition delay time of 60 ms, the turbulence level in the 20-liter sphere has a root-mean-square value which depends on the dust dispersion device. In case of the perforated Dispersion Ring, v'_{rms} is equal to 2.68 m s^{-1}. With the Rebound Nozzle and the Dahoe Nozzle v'_{rms} is respectively equal to 3.75 and 2.79 m s^{-1}.

When the standard 20-liter explosion sphere is operated according to the prescribed injection procedure for dust explosion testing, the turbulence intensity in the period from 60 to 200 ms after the very beginning of the air blast can be correlated by means of Equation (3), where the constant t_0 has a value of 60 ms for all three dust dispersion devices. The constants $v'_{\mathrm{rms}}{}^{\circ}$ and n assume respective values of 2.68 m s^{-1} and -1.49 for the Perforated Dispersion Ring, 3.75 m s^{-1} and -1.61 for the Rebound Nozzle, and 2.79 m s^{-1} and -1.52 for the Dahoe Nozzle.

The decay of turbulence in the 20-liter sphere was compared with the decay of grid generated turbulence and observed to behave in a distinct manner. While the decay of grid generated turbulence consists of two stages where the exponent, n, in Equation (3) assumes a constant value, namely, the initial and final period of decay, the decay of turbulence in the 20-liter sphere appears to have only one stage with a constant exponent. The value of this exponent is systematically different from those in the initial and final period of the decay of grid generated turbulence. The reason for this disparate behavior is ascribed to the fact that the turbulent fluctuations in the 20-liter sphere are created by a different mechanism (the baroclinic effect) than in the case of grid generated turbulence (friction).

It was mentioned in the Introduction that various researchers discussed the limitations of the cube-root-law and advocated its replacement by a more fundamental approach which takes the effect of turbulence explicitly into account. Since this approach involves the use integral balance models in conjunction with relationships that describe the turbulent flame propagation process in terms of laminar flame propagation parameters and the turbulence properties of the unburnt mixture ahead of the flame, accurate knowledge of both becomes of crucial importance. In practice, it is very difficult to stabilize a laminar dust flame in order to measure the laminar burning velocity and the laminar flame thickness. It is comparatively easy, however, to create turbulent dust explosions in laboratory test vessels, such as the 20-liter sphere, and to measure the behavior of the pressure as a function of time. When the turbulence properties in the test vessels are known at the moment of ignition, as well as during the course of the explosion, integral balance models can be fitted to the pressure-time recordings in order to determine the laminar burning velocity and the laminar flame thickness. In this respect, the decay law expression (3), with its parameters characterized for the three most widely used dust dispersion devices, will contribute to the establishment of a more fundamental approach to dust explosion severity prediction. Since correlations for the turbulent burning velocity and the turbulent flame thickness also involve the turbulence length scale, it is also important to investigate the behavior of this quantity in laboratory explosion vessels.

A comparison between the turbulence levels in the 20-liter sphere and the 1-m^3 vessel, based on our measurements, shows that equal turbulence levels exist in both vessels when the ignition delay time in the 20-liter sphere is equal to 200 ms. This result is consistent with the implication of the observations made by Pu et al., namely, that equal turbulence levels exist in both vessels when the ignition delay time in the 20-liter sphere is equal 200 ms. At the same time the result of this comparison contradicts van der Wel et al., who claim that similar conditions of turbulence exist in the two test vessels when the ignition delay time in the 20-liter sphere is equal to 165 ms.

As mentioned in the Introduction, Bartknecht and Siwek measured equal K_{St}-values in the 20-liter sphere and the 1-m^3 vessel. Apart from giving rise to the notion that equal turbulence levels exist in both test vessels at the prescribed igni-

tion delay times of 60 ms and 600 ms, their research also inspired the widespread belief that a formal cube-root-law agreement exists between dust explosion severities measured in the two test vessels. In addition to that, their research stimulated the use of the cube-root-law as a predictive tool which enables engineers to assess the severity of an industrial dust explosion on the basis of dust explosion severities measured in laboratory test vessels. Our measurements show that significantly different turbulence levels exist in the two test vessels at the prescribed ignition delay times. Hence, the results of Bartknecht and Siwek, which form the experimental basis of the cube-root-law, were obtained by igniting dust clouds under significantly different conditions of turbulence in the two test vessels. As a result the cube-root-law may not be considered as a generally valid. In fact, its use in the practice of scaling laboratory test results into what might happen during accidental industrial dust explosions must be regarded as fundamentally wrong. This conclusion supports the idea of abandoning the cube-root-law and replacing it with a more fundamental approach.

References

1. *Venting of Deflagrations*. NFPA 68, National Fire Protection Association (NFPA) (1988).
2. *Pressure Venting of Dust Explosions*. VDI 3673, Verein Deutscher Ingenieure (VDI), Düsseldorf (1995).
3. Bartknecht, W., *Dust Explosions: Course, Prevention, Protection*. Springer-Verlag, Berlin (1989). [Translation of *Staubexplosionen*, by R.E. Bruderer, G.N. Kirby and R. Siwek.]
4. International Standardization Organization (ISO), Explosion protection systems – Part 1: Determination of explosion indices of combustible dusts in air. ISO 6184/1 (1985).
5. Siwek, R., 20-l Laborapparatur für die Bestimmung der Explosionskenngrößen brennbarer Stäube. Ph.D. Thesis, Technical University of Winterthur, Winterthur, Switzerland (1977).
6. Van der Wel, P.G.J., van Veen, J.P.W., Lemkowitz, S.M., Scarlett, B. and van Wingerden, C.J.M., An interpretation of dust explosion phenomena on the basis of time scales. *Powder Technology* **71**(2) (1992) 207–215.
7. Pu, Y.K., Jarosinski, J., Johnson, V.G. and Kauffman, C.W., Turbulence effects on dust explosions in the 20-liter spherical vessel. In: *Proceedings of the Twenty-Third Symposium (International) on Combustion*. The Combustion Institute, Pittsburgh, PA (1990) pp. 843–849.
8. Eckhoff, R.K., *Dust Explosions in the Process Industries*, 2nd edn. Butterworth and Heinemann (1996).
9. Bradley, D., Chen, Z. and Swithenbank, J.R., Burning rates in turbulent fine dust-air explosions. In: *Proceedings of the Twenty-Second Symposium (International) on Combustion*. The Combustion Institute, Pittsburgh, PA (1988) pp. 1767–1775.
10. Dahoe, A.E., Zevenbergen, J.F., Lemkowitz, S.M. and Scarlett, B., Dust explosions in spherical vessels: The role of flame thickness in the validity of the 'cube-root-law'. *Journal of Loss Prevention in the Process Industries* **9**(1) (1996) 33–44.
11. Tamanini, F., Turbulence effects on dust explosion venting. *Plant/Operations Progress* **9**(1) (1990) 52–61.
12. Dahoe, A.E., Dust explosions: A study of flame propagation. Ph.D. Thesis, Delft University of Technology (2000).
13. Bradley, D. and Mitcheson, A., Mathematical solutions for explosions in spherical vessels. *Combustion and Flame* **26** (1976) 201–217.

14. Nagy, J. and Verakis, H.C., *Development and Control of Dust Explosions*. Marcel Dekker, New York (1983).

15. Perlee, H.E., Fuller, F.N. and Saul, C.H., Constant-volume flame propagation. Report of Investigations 7839, United States Department of the Interior, Bureau of Mines, Washington, DC (1974).

16. Chirila, F., Oancea, D., Razus, D. and Ionescu, N.I., Pressure and temperature dependence of normal burning velocity for propylene-air mixtures from pressure-time curves in a spherical vessel. *Revue Roumaine de Chimie* **40**(2) (1995).

17. Bradley, D., Lawes, M., Scott, M.J. and Mushi, E.M.J., Afterburning in spherical premixed turbulence explosions. *Combustion and Flame* **99** (1994) 581–590.

18. Tamanini, F., Modeling of turbulent unvented gas/air explosions. *Progress in Aeronautics and Astronautics* **154** (1993) 3–30.

19. Bradley, D. and Lee, J.H.S., In: *Proceedings of the First International Colloquium on the Explosibility of Industrial Dusts*, Volume 2 (1984) pp. 220–223.

20. Batchelor, G.K. and Townsend, A.A., Decay of vorticity in the isotropic turbulence. *Proceedings of the Royal Society of London, Series A: Mathematical and Physical Sciences* **190** (1947) 534–550.

21. Batchelor, G.K. and Townsend, A.A., Decay of isotropic turbulence in the initial period. *Proceedings of the Royal Society of London, Series A: Mathematical and Physical Sciences* **193** (1948) 539–558.

22. Batchelor, G.K. and Townsend, A.A., Decay of isotropic turbulence in the final period. *Proceedings of the Royal Society of London, Series A: Mathematical and Physical Sciences* **194** (1948) 527–543.

23. Van der Wel, P.G.J., Ignition and propagation of dust explosions. Ph.D. Thesis, Delft University of Technology, Delft, The Netherlands (1993).